Status of DIII–D Plasma Control*

M. Walker,[a] J.R. Ferron,[a] B. Penaflor,[a] D.A. Humphreys,[a] J.A. Leuer,[a] A.W. Hyatt,[a] C.B. Forest,[a]
J.T. Scoville,[a] B.W. Rice,[b] E.A. Lazarus,[c] T.W. Petrie,[a] S.L. Allen,[b] G.L. Jackson,[a] and R. Maingi[d]

[a]General Atomics, P.O. Box 85608, San Diego, California 92186-9784
[b]Lawrence Livermore National Laboratory, Livermore, California
[c]Oak Ridge National Laboratory, Oak Ridge, Tennessee
[d]Oak Ridge Associated Universities, Oak Ridge, Tennessee

ABSTRACT

A key component of the DIII–D Advanced Tokamak and Radiative Divertor Programs is the development and implementation of methods to actively control a large number of plasma parameters. These parameters include plasma shape and position, total stored energy, density, rf loading resistance, radiated power and more detailed control of the current profile. To support this research goal, a flexible and easily expanded digital control system has been developed and implemented [1]. We have made parallel progress in modeling of the plasma, poloidal coils, vacuum vessel, and power system dynamics and in ensuring the integrity of diagnostic and command circuits used in control. Recent activity has focused on exploiting the mature digital control platform through the implementation of simple feedback controls of more exotic plasma parameters such as enhanced divertor radiation, neutral pressure and Marfe creation and more sophisticated identification and digital feedback control algorithms for plasma shape, vertical position, and safety factor on axis (q_0). A summary of recent progress in each of these areas will be presented.

DIGITAL PLASMA CONTROL SYSTEM OVERVIEW AND PREVIOUS RESULTS

A flexible digital plasma control system (PCS) has been developed [1] and is now in routine use. The PCS computational hardware consists of SPARC Host computers, CSPI i860-based Supercard processors, and the GA-built Data Acquisition Daughterboard (DAD). Analog diagnostic measurements are brought from the tokamak to the PCS. Many of them are passed through analog anti-aliasing filters before being digitized for plasma control. A GA-built controller module requests conversion of analog signals to digital upon command from the PCS. This digitized data is buffered by the DAD before being passed to the Supercard(s) for processing. Realtime control algorithms which are part of the collection of PCS software execute to produce commands to be sent out to DIII–D actuators (power supplies, gas valves, etc.). The digital outputs of the Supercard comprise the commands sent to the D/A convertors and digital I/O board which in turn send analog and digital commands, respectively, to the various DIII–D actuators. Definition of plasma shape and shot evolution are accomplished by the physics operator using the PCS graphical user interface.

A description of the digital control software which executes on this platform is given in [2].

The PCS supports a wide variety of plasma shapes and experimental controls during operations. So far, 12 different shapes have been produced using the PCS including double-null, single-null, limiter, as well as shapes designed to match ITER, JET, and C-MOD.

Several "first of their kind" results were accomplished with early versions of the PCS hardware/software. These include control of total stored energy by pulse width modulation of injected neutral beam power [3,4], minimization of rf loading resistance by control of antenna-to-plasma gap [3], and feedback control of error fields using saddle coils [5,6]. Control algorithms which predated the PCS such as density control were also converted to run with the digital system.

Preliminary results of multivariable modeling, experimental model validation, and control analysis of the plasma, poloidal coils, vacuum vessel, and power system dynamics have also been previously reported [7].

RECENT WORK

R recent control work at DIII–D has focused on development and implementation of hardware and software tools and control models necessary to support advanced control. This includes expansion of the PCS to three realtime CPUs, a major upgrade to version 10 of the PCS software, installation of the PCS software on two additional control platforms — a software development and test system without data acquisition capability and a full hardware/software implementation for control of rf transmitters. A version of the PCS hardware/software is also used for data acquisition for the Charge Exchange Recombination diagnostic. The DIII–D plasma discharge control PCS presently acquires 184 diagnostic input channels and has 38 output channels (commands to actuators). Programmable bandwidth anti-aliasing filters have been installed on 128 of the real-time diagnostics.

Extensive work has been done in areas which support modern control. All coil/vessel systems and power systems have been modeled and validated with experimental test data [8]. Linear, nonrigid, flux-conserving models of plasma dynamics

are now being generated on a routine basis using the LLNL Corsica code [9]. The dominant modes of these models (corresponding to radial and vertical motion) have been validated against DIII–D experimental data. Systematic calibration procedures are being implemented to ensure the integrity of diagnostic and command circuits used in control [10]. Work continues on refining algorithms for plasma parameter estimation, and developing control of actuators — specifically the shape control power supplies. This power supply control is described below.

Parallel work on simple controls of more exotic parameters has exploited the existing digital control capability. Some examples of this are described below.

A. *Digital Vertical Position Control*

The present analog plasma vertical position (z) control is now being implemented as a digital algorithm in the PCS. Operational experience has shown this control to be effective and robust. It has already been characterized in terms of its frequency response and implemented in digital code. In the present analog vertical control, a computed value of error between desired z position and estimated z position is passed through a pair of analog filters to produce quantities known as verta and vertb [11]. These quantities are scaled and added to the commands for the poloidal shaping coils (F-coils) 2A, 2B, 6A, 6B, 7A, and 7B. Fig. 1 shows the fit to the analog frequency response for verta obtained by combining the frequency response of analog anti-aliasing filters on the magnetic diagnostics used to estimate z position with a digital filter on the vertical position error implemented in the PCS. This comparison assumes a particular implementation with a computational cycle time of 60 µs. The ordinate of
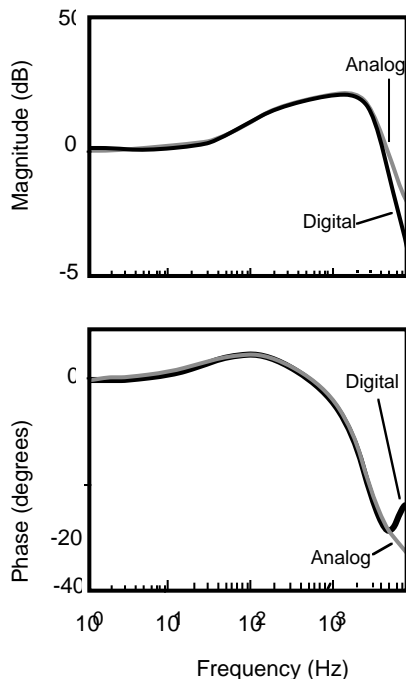
the plot stops at the Nyquist frequency of 8.333 kHz for this cycle time.

The digital calculation (no feedback) of the quantities verta and vertb has been implemented and tested during operations. Computational cycle time was ≈60 µs.

B. *Multivariable Shape Control*

Multivariable shape controllers have been designed and tested in simulation for both DIII–D and ITER. The DIII–D controllers have not yet been implemented because virtually all multivariable plasma controllers assume well-controlled input actuators (for example, voltages across coils). In the case of shape control, the DIII–D actuators are pulse width modulated (PWM) power supplies known as choppers which modulate an approximately constant voltage from 12-pulse power convertors known as F-supplies. Choppers presently produce output voltage which is not feedback regulated and which varies nonlinearly with F-coil current, F-supply voltage, and command voltage.

Feedback control of chopper voltage has been implemented and tested experimentally. Fig. 2 shows a plot of voltage demand versus lowpass filtered chopper voltage for one chopper during shot 83107. The voltage data was lowpass filtered to remove the high frequency PWM signal although some residual "noise" from this modulation can still be seen in the plots. The chopper was turned on at approximately –0.70 s and the control algorithm was turned on at approximately –0.68 s. There is a small offset in acquired data evident in the plot due to the acquisition circuit. Tracking accuracy for the tests conducted was typically within about 5% — adequate for the intended application as voltage sources for a multivariable controller. Voltage control of choppers is now being implemented as a standard option in the PCS.

C. *Safety Factor on Axis*

Control of the current density (or *q* profile) has been proposed as a method for improving confinement and β for advanced tokamaks. This requires real-time diagnostic measurements, algorithms to compute the *q* profile from diagnostic inputs, and non-inductive current drive sources to

Fig. 1. Comparison of existing analog verta filter frequency response with response of combined anti-aliasing and digital filters.
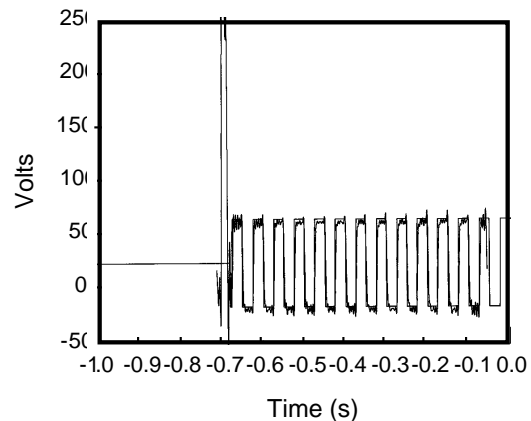

Fig. 2. Comparison of filtered acquired chopper voltage with demand voltage.

modify the q profile. The primary instrument on DIII–D for measurement of q profiles is the Motional Stark Effect (MSE) diagnostic. MSE data is now acquired routinely on DIII–D by the real-time control computer and by the diagnostic acquisition system. A simple real-time algorithm to calculate q_0 has been developed and tested during a sawtoothing H–mode discharge. We are prepared for the initial tests of q_0 feedback control with Fast Wave Current Drive (FWCD). As the current drive sources such as FWCD and electron cyclotron current drive become available at higher power over the next several years, we will be in a position to control other details of the q profile such as the value and radius of q_{min} in reverse shear configurations.

Our long term goal is development of a fast algorithm to calculate the complete q profile from MSE and magnetic input data. This problem is very complex on a shaped, high-β tokamak like DIII–D. A simple relationship between q_0 and the MSE pitch angle (B_p/B_t) measurements is given by $q_0 \approx \kappa_0/R_0 (\partial \gamma_t/\partial R)_0$ where R_0 is the magnetic axis radius, κ_0 is the elongation on axis, $\gamma_t = (A_1/A_2) \tan, \gamma, \gamma$ = measured pitch angle, and A_1, A_2 are geometric constants. Both R_0 and γ_t are obtained directly from the MSE measurements. So if κ_0 can be estimated, then the calculation of q_0 is quite straightforward. κ_0 depends most significantly on external shape, the current density on axis, and beta poloidal. In practice, for monotonic q profiles with $1 < q_0 < 2$, κ_0 does not vary over a large range and a fixed estimate can be used.

During the real-time test, the control computer was performing shape control and calculating q_0 in parallel (no feedback on q_0). The q_0 calculation takes about 600 μs to execute; this speed is more than adequate for real-time control applications. Excellent agreement is observed between real-time calculated values of q_0 and values from the EFIT equilibrium code shown in Fig. 3. The value of κ_0 is about 1.35 in this case, giving q_0 =0.9 to 0.95.

D. *Optimization of Plasma Breakdown/Startup*

During 1995, a leak was found in a lead to a portion of the Ohmic heating solenoid (E-coil). A decision was made to disconnect and operate without the affected portion. This new E-coil configuration required a change in methods used for plasma breakdown. The effects of the E-coil change relevant to startup were: non-zero B_r produced by the new configuration, nonsymmetric coils top and bottom, fewer available volt-seconds, and outer F-coil current requirements lower than previously achievable.

A formal analysis was undertaken to determine optimum breakdown parameters for the new configuration. Important to breakdown and plasma operation is the creation of a large low field region and minimization of flux dissipation during plasma formation. A new control algorithm was developed specifically for the startup phase of the plasma discharge. This algorithm was able to produce good plasma breakdown on the first day of operation, even with outer F-coil current constraints imposed by their power supplies. These constraints were later removed with power supply modifications.
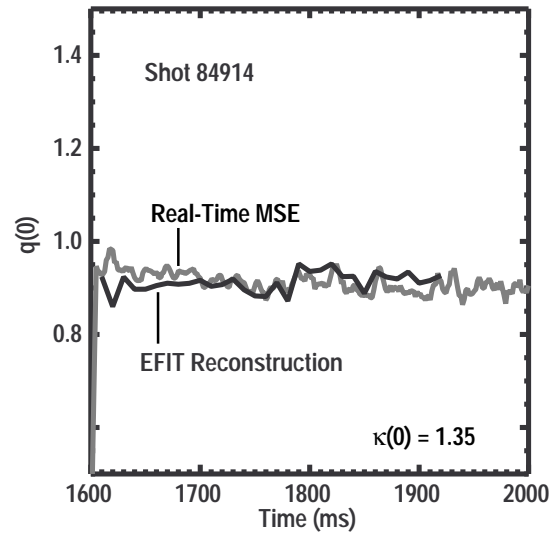

Fig. 3 DIII–D digital plasma control system provides real-time calculation of q_0

Optimum startup occurs when there is a large region of low $|B|$, sufficient voltage to cause Townsend avalanche and impurity burn through, and correct field curvature to produce a stable plasma following the avalanche. Prior to the E-coil modifications, the up/down symmetry of the system guaranteed low radial error fields $B_r \approx 0$ in the breakdown region. The outer F-coils (F6A, F6B, F7A, F7B) were programmed to buck out the small vertical field B_z generated in the plasma region by the E-coil during the pre-biasing of the coil and that contributed by eddy currents in the vacuum vessel. (See Fig. 4.)

The new E-coil configuration in DIII–D requires us to minimize B_r as well as B_z to achieve good startup. In addition, once breakdown occurs we must produce the correct field curvature to ensure stable plasma formation. This is characterized by the decay index, $n \equiv -R/B_z (\partial B_z/\partial R)$ which must be in the range $0 < n < 1.5$ for stable operation [17]. Using the four outer coils, solutions can be found which compensate to second order in the multipole expansion of B_z and first order in B_r.

The real-time control algorithm solves the equations

$$\vec{Q}_1^z \cdot \left(\vec{i}_e + \vec{i}_f\right) = B_z \quad , \tag{1}$$

$$\vec{Q}_1^r \cdot \left(\vec{i}_e + \vec{i}_f\right) = 0 \quad , \tag{2}$$

$$\vec{Q}_2^z \cdot \left(\vec{i}_e + \vec{i}_f\right) = 0 \quad , \tag{3}$$

for the outer F-coil currents at approximately –100 ms. Eq. (1) represents the vertical field dipole moment, (2) represents the radial field dipole moment, and (3) represents the vertical field quadrupole moment, where $\vec{i}_e$ is the current in the E-coil and $\vec{i}_f$ is the current in the outer F-coils. All expansions are at a pre-specified desired null radius R_{null}. Using the fact that

$$n = -2R \left[\vec{Q}_2^z \cdot \left(\vec{i}_e + \vec{i}_f\right) \right] / \left[\vec{Q}_1^z \cdot \left(\vec{i}_e + \vec{i}_f\right) \right]$$
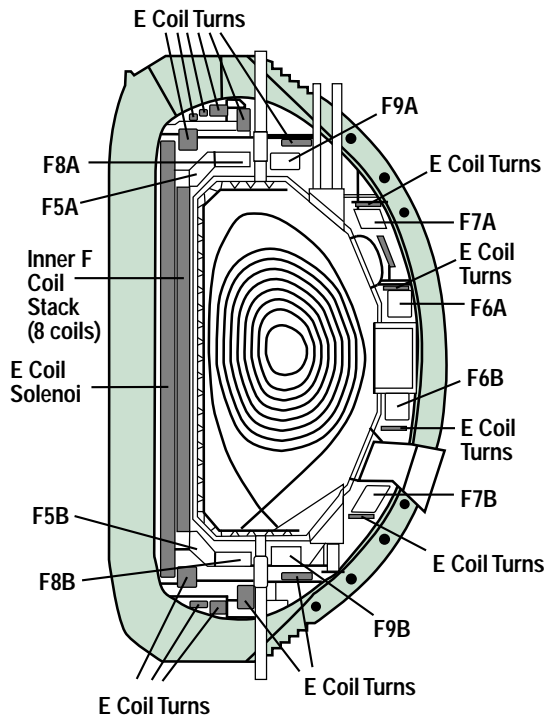
Fig. 4. DIII–D cross-section showing placement of E-coil turns and outer F-coils 6A, 6B, 7A, and 7B.

we are able to null B_r and n, and achieve a pre-specified (small) B_z. The extra degree of freedom given by having four outer F-coils is used to choose the solution which maximizes the minimum F-coil current.

E. *Radiated Power Control*

Puffing of D_2, neon, argon, and nitrogen gas has been used successfully in experiments to reduce divertor peak heat flux in H–mode plasmas [12–14]. These "radiative divertor" experiments were directed toward addressing the problem of unacceptably high heat loading at the divertor plates anticipated for next generation tokamaks such as ITER.

When cold deuterium gas is injected into ELMing H–mode plasmas in DIII–D, hydrogenic radiation, intrinsic impurity radiation, and charge-exchange radiation in the divertor region increase, which causes a significant reduction both in the *peak* heat flux on the divertor tiles ($\hat{q}_{div}$) and in the total power measured at the divertor tiles (P_{div}). After a sufficient amount of deuterium gas has been added to the system however, a high density, highly radiative region forms between the outboard separatrix strike point location and the X-point and its appearance is concurrent with a pronounced further drop in $\hat{q}_{div}$ and P_{div}. The largest reductions in peak heat flux and power flow at the divertor target occur at this time. This operating regime is referred to as the Partially Detached Divertor (PDD). The term "partially" implies that particle and heat fluxes are not driven to zero everywhere on the strike plate. Experiments have shown that further reduction in either $\hat{q}_{div}$ or P_{div} by continued D_2 puffing at a steady high rate is relatively small. Moreover, "overpuffing" often results in an unacceptable rise in central density coupled with significant degradation in the energy confinement time τ_E. Consequently, it would be optimal to inject only the minimal neutral gas necessary to maintain the PDD regime.

Experimentally, PDD operation has been maintained without overpuffing by feedback on midplane neutral pressure $\left(p0_{mid}\right)$ [12]. A very simple algorithm is used: if the midplane neutral gas pressure $p0_{mid} \leq 0.3$ mTorr, D_2 gas was injected at a prescribed rate to raise $p0_{mid}$ above 0.3 mTorr; if $p0_{mid} > 0.3$ mTorr, D_2 injection was turned off. (It had been determined in experiments that $p0_{mid} \approx 0.3$ mTorr was at the boundary between initiating (and suppressing) PDD activity at the specified input power.) This approach was successful in arresting the steady rise in the line-averaged density of the main plasma.

A more complicated algorithm has been successfully used for experiments requiring constant edge plasma radiated power by feedback control of the rate of impurity gas injection. Approximate radiated power is derived by taking the derivative, smoothing, and then summing the input signal from four selected channels of the 48 channel bolometer diagnostic. The radiated power is then compared with the desired value and the resulting error signal is processed by a standard PID module in the PCS. The output of this module controls an impurity gas injection valve. The impurity gas, typically neon, was chosen so that the spectral line radiation occurs primarily in the edge plasma region.

Experiments have also been performed which combine divertor heat flux reduction and density control using divertor pumping. A PDD discharge [15] has been sustained with puffing and divertor pumping for the duration of the D_2 gas pulse, ≈ 2 s. The effective pumping speed of the divertor cryopump is controlled by the location of the outboard separatrix strike point. The exhaust rate (180–240 Torr l/s) nearly matched the gas fueling rate (220–230 Torr l/s), so the core plasma density was held nearly constant. This was a high quality ELMing H–mode [$\tau_E \approx 2 \times \tau$(ITER89)], with a very modest decrease in τ_E due to the gas puff. Divertor pumping also improves the quality of control of edge radiated power using impurity gas injection.

REFERENCES

[1] J.R. Ferron, *et al.*, in Proc. of IEEE Symp. on Fusion Engineering, pp. 761–764, 1992.
[2] J.R. Ferron, *et al.*, "A flexible software architecture for tokamak discharge control systems," this conference.
[3] G.L. Campbell, *et al.*, .in Proc. of 17th Symp. on Fusion Technology, pp. 1017–1021, 1992.
[4] T.S. Taylor, *et al.*, in Proc. of 14th Inter. Conf. on Plasma Physics and Contr. Nucl. Fusion Research, pp. 167–180, 1992.
[5] R.J. La Haye and J.T. Scoville, "First results from the C-coil," General Atomics Report C21897, 1994.
[6] R.J. La Haye, T.E. Evans, J.T. Scoville, "Experiments on plasma rotation control with C-coil," General Atomics Report C22009, 1995.
[7] M. Walker, D.A. Humphreys, A. Nerem, in Proc. of 15th IEEE Symp. on Fusion Engineering, pp. 235–241, 1993.
[8] M. Walker, A. Nerem, D. Baggest, "Advanced plasma control system models for feedback control," General Atomics Report GA-A21745 (1995).
[9] L.D. Pearlstein, S.W. Haney, and J.A. Crotinger, Livermore National Laboratory private communication August 1995.
[10] D. Baggest, *et al.*, "Improving plasma shaping accuracy through consolidation of control model maintenance, diagnsotic calibration, and hardware change control," this conference.
[11] E.A. Lazarus, J.B. Lister, G.H. Neilson, *Nucl. Fusion* **30**, p. 111, 1992.
[12] T.W. Petrie, *et al.*, "Radiative divertor experiments in DIII–D with D_2 injection," General Atomics Report GA-A21879, 1994.
[13] S.L. Allen, *et al.*, "*J. Nucl. Mater.* **220–222**, p. 336, 1995.
[14] M.J. Schaffer, *et al.*, "Impurity Reduction During 'puff and pump' experiments on DIII–D," to be published in Nucl. Fusion.
[15] D.N. Hill, *et al.*, "Divertor research on the DIII–D tokamak," to be published in Plasma Phys. and Contr. Nucl. Fusion.
[16] V.S. Mukhovatov, V.D. Shafranov, *Nucl. Fusion* 11, p. 605, 1971.